



## Letter

**Cite this article:** Schaap T, Roach MJ, Peters LE, Cook S, Kulesa B, Schoof C (2020). Englacial drainage structures in an East Antarctic outlet glacier. *Journal of Glaciology* 66(255), 166–174. <https://doi.org/10.1017/jog.2019.92>

Received: 1 July 2019

Revised: 11 November 2019

Accepted: 12 November 2019

First published online: 23 December 2019

**Key words:**

Glacier geophysics; glacier hydrology; ground-penetrating radar

**Author for correspondence:**

Thomas Schaap,

E-mail: [thomas.schaap@utas.edu.au](mailto:thomas.schaap@utas.edu.au)

# Englacial drainage structures in an East Antarctic outlet glacier

Thomas Schaap<sup>1</sup> , Michael J. Roach<sup>1</sup> , Leo E. Peters<sup>2</sup> , Sue Cook<sup>3</sup> , Bernd Kulesa<sup>4,5</sup>  and Christian Schoof<sup>6</sup>

<sup>1</sup>Discipline of Earth Science, University of Tasmania, Hobart, Tasmania 7001, Australia; <sup>2</sup>Seismic Research Centre, The University of the West Indies, St. Augustine, Trinidad and Tobago, West Indies; <sup>3</sup>Institute for Marine and Antarctic Studies, University of Tasmania, Private Bag 129, Hobart 7001, Australia; <sup>4</sup>Glaciology Group, College of Science, Swansea University, Singleton Park, Swansea SA2 8PP, UK; <sup>5</sup>School of Technology, Environments and Design, University of Tasmania, Hobart, Tasmania 7001, Australia and <sup>6</sup>Department of Earth and Ocean Sciences, University of British Columbia, Vancouver, British Columbia, Canada

**Abstract**

Ground-penetrating radar data acquired in the 2016/17 austral summer on Sørsdal Glacier, East Antarctica, provide evidence for meltwater lenses within porous surface ice that are conceptually similar to firn aquifers observed on the Greenland Ice Sheet and the Arctic and Alpine glaciers. These englacial water bodies are associated with a dry relict surface basin and consistent with perennial drainage into an interconnected englacial drainage system, which may explain a large englacial outburst flood observed in satellite imagery in the early 2016/17 melt season. Our observations indicate the rarely-documented presence of an englacial hydrological system in Antarctica, with implications for the storage and routing of surface meltwater. Future work should ascertain the spatial prevalence of such systems around the Antarctic coastline, and identify the degree of surface runoff redistribution and storage in the near surface, to quantify their impact on surface mass balance.

**Introduction**

Englacial channels represent current and relict flow pathways for meltwater through the body of a glacier (Gulley and others, 2009). They can provide pathways for surface water to reach the bed of a glacier and can affect its dynamics by altering the subglacial hydrological system (Fountain and Walder, 1998; Zwally and others, 2002; Schoof, 2010).

Englacial channels have been observed to form by three main mechanisms: (a) ‘cut-and-closure’, (b) exploitation of permeable structures and (c) hydrofracture of crevasses (Gulley and others, 2009). The cut-and-closure formation mechanism described by Gulley and others (2009) occurs where supraglacial streams incise into the ice through melting, and the upper portion of the resulting canyon closes through ice creep. Systems which form by this mechanism are characterised by meandering channels with a low gradient and occasional step-pools. This mechanism requires the downcutting rate of the stream to be higher than the ablation rate of the surrounding ice, with this mechanism being most common in regions of low surface ablation and high stream flow rates (i.e. high surface slope and large catchment areas), and has typically been observed in glaciers at high latitude (Gulley and others, 2009; Vatne and Irvine-Fynn, 2016; Benn and others, 2017).

Shreve (1972) proposed a different model involving pre-existing permeable structures, such as veins in the ice, which are exploited and enlarged. However, the primary porosity and hence hydraulic conductivity of glacier ice is extremely low. Secondary porosity created by relatively permeable macro-structures, such as debris layers or fractures, is therefore a more plausible mechanism. These permeable pathways are expanded by the transfer of heat from meltwater passage into conduits. The morphology of these conduits depends on their origin, and conduits which encounter crevasses can have pronounced morphological undulations (Gulley and others, 2009).

The hydro-fracture model provides an efficient drainage pathway through the entire ice thickness using pre-existing surface crevasses. The depth of surface crevasses is normally limited by the closing action of ice creep. However, if a surface crevasse is water-filled, the additional pressure counteracts the ice overburden pressure and allows the crevasse to deepen. If the surface of the water body contains a sufficient volume, the crack will quickly deepen through the entire ice thickness (Weertman, 1973; van der Veen, 2007). This mechanism allows the rapid drainage of surface melt lakes in Greenland (Das and others, 2008; Doyle and others, 2013; Jones and others, 2013) and on Antarctic ice shelves (Scambos and others, 2009). Hydro-fracture produces shafts with a plunge angle that is dependent on the local stress regime (Gulley and others, 2009) and can also lead to a permanent connection between an ice-sheet surface and bed in the form of a moulin (Alley and others, 2005).

Englacial channels have been directly observed and geophysically detected in cold-based (Vatne, 2001), temperate and polythermal (Stuart and others, 2003; Catania and others, 2008; Benn and others, 2017) glaciers from Greenland, Svalbard and the Himalaya. Englacial meltwater accumulations have also been described in East Antarctica (Lenaerts and others, 2016). Ground-penetrating radar (GPR) detection of englacial channels has

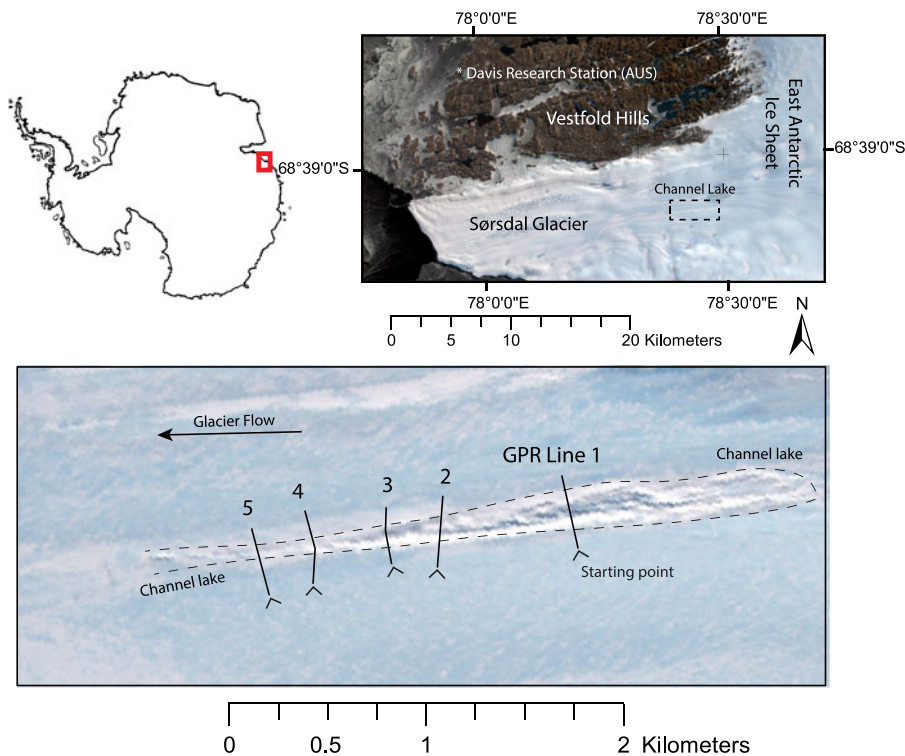


**Fig. 1.** Maps showing the location of Sørsdal Glacier and Channel Lake with GPR transects (solid black lines labelled 1 to 5). Base imagery captured 29th March 2017 by Sentinel 2 satellite.

been noted as far south as King George Island, near the Antarctic Peninsula (Kim and others, 2010; da Rosa and others, 2014). Few direct and indirect observations of englacial hydrological systems have been reported from Antarctica (e.g. Langley and others, 2016), and GPR observations of near-surface drainage systems in Antarctica have not yet been reported.

Surface meltwater is visible in satellite imagery around much of Antarctica (Kingslake and others, 2017). This meltwater is typically contained in surface melt ponds, or drains supraglacially in streams over the ice-sheet surface. Surface melt ponds have been associated with rapid ice-shelf retreat (e.g. Scambos and others, 2009), with the rapid simultaneous drainage of multiple surface melt ponds being suggested as the trigger for collapse (Banwell and others, 2013; Macayeal and Sergienko, 2013). Surface water drainage has also been put forward as an explanation for surface structures known as ‘ice dolines’ (Bindschadler and others, 2002). Ice dolines are large, steep-sided depressions that have been observed on the surface of ice shelves, and have been suggested to form as englacial water bodies drain, allowing the surface of the ice to collapse (Mellor, 1960).

Here we present GPR observations that indicate the presence of a near-surface englacial drainage system in the Sørsdal Glacier, Princess Elizabeth Land, East Antarctica, and use forward models of electromagnetic wave propagation to characterise the englacial channel contents.

### Study area

Sørsdal Glacier is a major outlet of the East Antarctic Ice Sheet, flowing adjacent to the Vestfold Hills in Princess Elizabeth Land (Fig. 1). The floating section of the glacier is ~20 km long and a maximum of 10 km wide. Sørsdal Glacier experiences significant surface melt in the austral summer, resulting in the seasonal development of surface meltwater ponds.

This study focuses on a single surface feature in the ablation zone of Sørsdal Glacier, which we have informally named ‘Channel Lake’. In February 2017, when fieldwork for this study was conducted, Channel Lake was characterised by an elongate, mostly dry surface basin. The surface consisted of solid ice with

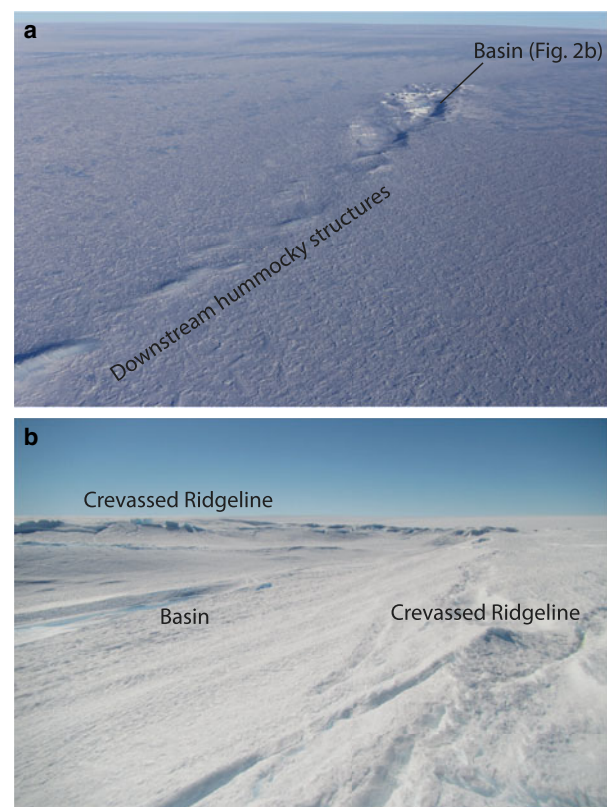


**Fig. 2.** (a) Photograph of Channel Lake taken from a helicopter, looking northeast. Channel Lake and its associated downstream structures are together ~4 km in length; (b) photograph of Channel Lake basin looking east from the southern ridge. Here, the bounding ridges are up to 10 m high and are ~100 m apart. Both photographs were taken during summer 2016/17.

meltwater puddles scattered across. No snow or firn was observed from the surface or in shallow (<1 m) boreholes drilled with a hand auger. Raised hummocky features were seen on the glacier surface, appearing as a down-glacier continuation of Channel

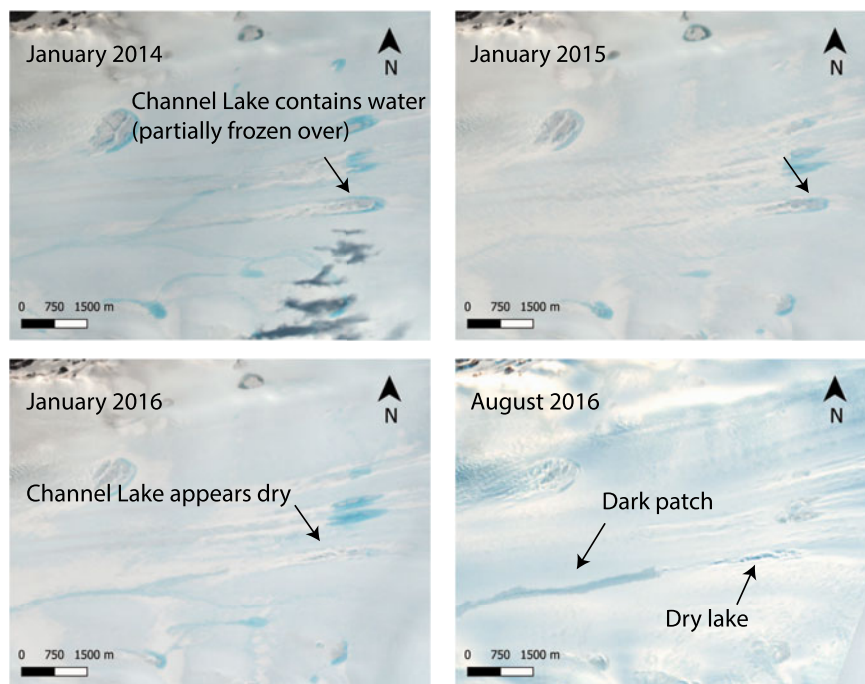


**Fig. 3.** Satellite imagery (Landsat 8 OLI/TIRS C1 Level 1) showing the evolution of Channel Lake on Sørsdal Glacier between 2014 and 2016.

Lake (Fig. 2a). The basin itself was bordered by steep, crevassed ridges, similar to those observed in ice dolines (Bindenschadler and others, 2002) (Fig. 2b). Channel Lake was located  $\sim 22$  km up-glacier of the calving front and  $\sim 1$  km up-glacier of the grounding line. Seismic reflection data (gathered supplementary to this study) from Channel Lake showed the ice was  $\sim 1400$  m thick. The Channel Lake basin formed a topographic depression  $\sim 10$  m below the surrounding glacier surface at its deepest point and extended  $\sim 4$  km along-flow (including associated downstream structures) and  $\sim 200$  m across. The average speed of the ice in the Channel Lake area is  $290 \text{ m a}^{-1}$  calculated using velocity data from MEaSUREs v2 (Rignot and others, 2017).

Channel Lake is similar to features that have previously been associated with surface lake drainage in East Antarctica (Langley and others, 2016). In satellite imagery taken from the 2014 and 2015 austral summers, Channel Lake can be seen as a supraglacial lake filled with water (Fig. 3). The area of the water-filled lake was  $\sim 0.6 \text{ km}^2$  in January 2014, although there is high uncertainty in this estimate due to difficulty in determining lake boundaries given that it was partially ice-covered. This water seems to have disappeared between January 2015 and January 2016, with the January 2016 image showing a dry basin similar to that encountered during our fieldwork in the 2016/17 austral summer. Furthermore, a satellite image from August 2016 shows a long, dark-coloured patch extending down-glacier of Channel Lake (Fig. 3). This dark region may be the manifestation of a refrozen accumulation of meltwater at the surface or near-surface. The drainage of Channel Lake and the emergence of water at the surface some distance down-glacier alludes to the possibility of a near-surface englacial drainage system which transported the water from Channel Lake to its re-emergence downstream. Here we investigate whether the features observed in satellite imagery can be associated with and hydrologically connected to englacial drainage pathways.

## Methods

### GPR acquisition

GPR data were collected in February 2017 across five transects: four across the basin feature of Channel Lake, and one

**Table 1.** Sampling parameters for GPR data on Sørsdal Glacier

Transmitted signal frequency	250 MHz	800 MHz
Time window	800 ns	256 ns
Samples per trace	2024	2024
Sampling frequency	2.5 GHz	7.9 GHz
Horizontal sample interval	5 cm	5 cm

downstream on flat ice (Fig. 1). Each transect was repeated with 800 and 250 MHz MALA Ramac antennas connected to a MALA X3Mc control system. Table 1 describes the sampling parameters for each antenna.

The GPR data were acquired by manually towing the antennas across the ice surface. The GPR transects were oriented orthogonally to the long axis of Channel Lake, with an approximate north-south orientation, and were numbered 1–5 from east to west; up-glacier to down-glacier (Fig. 1). The surface topography presented a significant challenge in the eastern transects (Lines 1–3) due to steep embankments littered with cracks and crevasses that made it difficult to maintain the antennas parallel to the surface and directly along the profiles at times leading to a minor loss of data on some profiles. The 800 MHz data on Line 5 suffered the most, where a degraded connection to the antenna severely degraded the quality of the data to the point of being unintelligible. Location data were gathered by handheld GPS devices.

### GPR processing

We opted for a minimalistic processing flow to minimise the distortion of signal attributes. A dewow filter was applied to each profile to remove inherent electronic noise, and a manual time-varying gain function amplified low-amplitude features at depth. This gain was only applied to help identify features, and was subsequently removed to preserve original signal characteristics for analysis. The profiles were then time-migrated using a well-known phase-shift algorithm (Stolt, 1978) to collapse diffractions and correct for dipping reflectors. In Figure 4, the radar-grams along Lines 1–3 are then displayed with a static correction of relative changes in topography, based on in-field



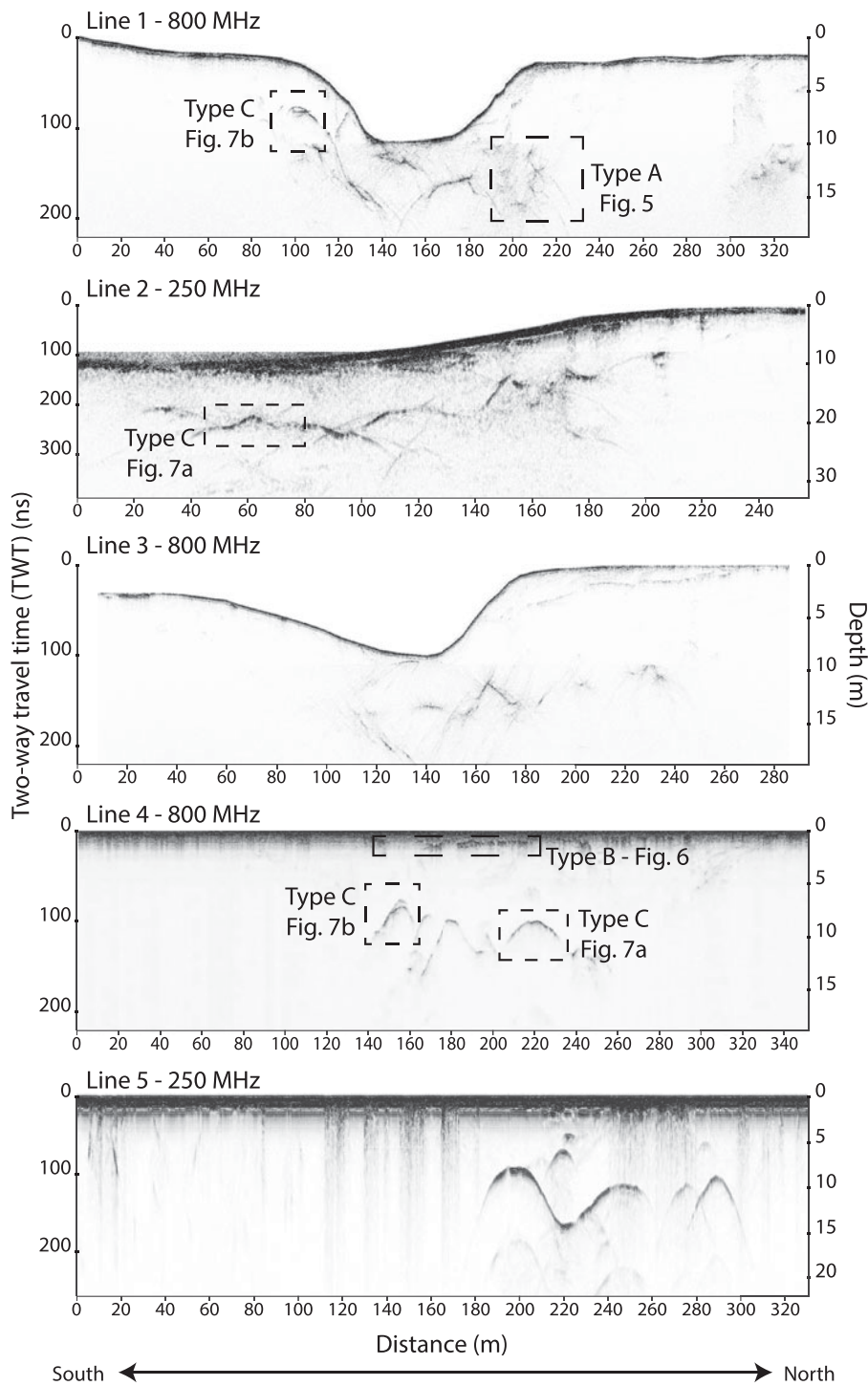


**Fig. 4.** GPR radargrams (locations shown in Fig. 1). Examples of each geometric class are annotated. Note the differences in scale and surface topography.

GPS observations with an estimated average vertical precision of  $\pm 0.5$  m. The surface topography of Lines 4 and 5 was flat without noticeable undulations.

#### Forward modelling

We consider a system of ice, air and water, with relative dielectric constants ( $\epsilon_r$ ), electrical conductivities ( $\sigma$ ), electromagnetic velocities and magnetic permeabilities ( $\mu_r$ ) taken from Plewes and Hubbard (2001) (Table 2). In situ observations from shallow augering around Channel Lake only identified the presence of ice, air and water, with no evidence of firn or snow.

The construction and interpretation of the forward models followed a similar methodology to that described by Stuart and others (2003). Models were constructed in a 2-D space; however,

they were only varied on the depth axis and not on the horizontal, and the boundary conditions were set to absorb all electromagnetic energy. This was done to facilitate a controlled forward model environment, avoiding the signal arising from non-horizontal reflectors which would otherwise interfere with the reflection signal from the interface being analysed. Three main types of model were tested, simulating different materials within a pocket in ice: air, water and air on top of water. For each model, a series of depths and thicknesses were tested for the pockets, and differing water/air thicknesses were tested in the case of the air-on-water model. Zero-offset traces were calculated by finite differencing of electromagnetic energy propagating vertically downwards from a 250 MHz Ricker wavelet source at the transmitter location, with a time step of 0.02 ns and a time window of 400 ns. The output of this process was a radargram

**Table 2.** Input properties of the modelled materials, taken from Plewes and Hubbard (2001)

Material	Relative dielectric constant ( $\epsilon_r$ )	Electrical conductivity ( $\sigma$ , mS m <sup>-1</sup> )	Relative magnetic permeability ( $\mu_r$ )	Velocity (m ns <sup>-1</sup> )
Ice	3	0.01	1	0.173
Water	80	0.5	1	0.033
Air	1	0	1	0.3

which was analysed in a manner similar to real data, with the exception that the forward-modelled data did not require any additional signal processing.

The amplitude of signals reflected from interfaces between different media is determined by the amplitude reflection coefficient ( $R$ ). These values may be used to infer the interfacing materials which produce reflections in GPR data. Five separate possible interfaces were considered in this study: ice over water, ice over air, air over ice, air over water and water over ice. Table 3 lists the calculated amplitude reflection coefficients of these interfaces as calculated using Eqn (1):

$$R = \frac{\sqrt{\epsilon_1} - \sqrt{\epsilon_2}}{\sqrt{\epsilon_1} + \sqrt{\epsilon_2}}, \quad (1)$$

$\epsilon_1$  and  $\epsilon_2$  are the dielectric constants of the overlying and underlying media respectively, assuming  $\mu_r \approx 1$  for each medium (Ward and Hohmann, 1987).

From these values, we can expect strong reflection signals from interfaces involving water and moderate reflections from interfaces of air. In practice, deducing the exact materials from reflection signals in glacier GPR data is challenging without precise knowledge of source wavelet properties or in situ observations to correlate with (e.g. ice cores intersecting features found in GPR data). The most powerful diagnostic for our purpose of identifying the nature of the englacial reflections is therefore the polarity of the reflections' first peaks, with the amplitude (often referred to as 'brightness' in GPR data) of the reflections only assessed in a relative sense. The presence of water is therefore indicated by bright reflectors with a negative peak polarity.

## Results

The GPR transects across Channel Lake showed multiple irregular subsurface features in every transect (Fig. 4). The highest spatial density of subsurface features is apparent underneath Channel Lake, with fewer features apparent to the north and south. The features occur mostly within 5–10 m of the surface and have horizontal extents from <1 m to over 50 m. Some radargrams also revealed horizontally extensive reflectors within the top 2 m. Within any given transect, some features are discrete, while others appear either interconnected or too close together to adequately resolve (Fig. 4).

We classify the features according to their geometries, identifying three main categories that are labelled A, B and C in Figure 4. Type A features are characterised by hyperbolae that are abundant in the unmigrated data and were observed on most profiles in groups beneath the margins of Channel Lake (e.g. Fig. 5). Type B features appear as bright, flat and laterally extensive reflections, and are particularly abundant in Lines 3 and 4 at shallow depths of <5 m (e.g. Fig. 6). Type C features encompass a broad range of bright, undulating, horizontally extensive reflections, and are observed in all radargrams in this study at depths typically exceeding 5 m (e.g. Fig. 7).

**Table 3.** Amplitude reflection coefficients for the various interfaces calculated from Eqn (1) and the material properties in Table 2

Interface	Amplitude reflection coefficient ( $R$ )
Ice–air	+0.27
Ice–water	−0.68
Air–ice	−0.27
Air–water	−0.80
Water–ice	+0.68

The forward models simulated single englacial pockets at varying depths, ranging from completely water-filled to completely air-filled, and combinations of the two. Consistent with our expectations, we simulated stronger reflections from ice–water or air–water interfaces than ice–air interfaces and confirmed the polarity of the reflections' first peaks being robustly diagnostic of the interface type (Table 3). No clear reflections were simulated for water–ice interfaces, in agreement with Stuart and others' (2003) inferences for englacial channels in a cold-ice Svalbard glacier, which implies that volume estimates of water-bearing englacial voids cannot readily be inferred from our GPR data. The vertical resolution of GPR data (i.e. the vertical distance between which two signals can be separable) is theoretically limited to a quarter of its pulse wavelength (Reynolds, 2011), and the skin depth of the signal is a function of its frequency and the conductivity of the medium. The estimates presented by Table 4 show that most reflection features in this study lie within the skin depth of ice for both antenna frequencies, and while the thickness of water bodies may be indeterminable, our 800 MHz should resolve an air pocket thicker than ~0.1 m. However, these values are only theoretical calculations based on the idealistic electrical parameters described in Table 2. It is likely that the vertical resolution of each system is in fact coarser, although this is difficult to quantify without in situ testing. Additionally, the skin depth in ice may vary significantly depending on the water content.

## Discussion

Type A features were mainly found underneath the crevassed ridges at the edges of the Channel Lake basin, and therefore likely represent small englacial crevasses or fractures. Type B reflections are flat, lie within 5 m of the surface and often extend over 20 m along transects. The reflection signal characteristics of Type B features are difficult to distinguish as a result of interference with noise at early two-way travel times; however, their high brightness and comparison to the model traces suggest these are indicative of water (Fig. 6). These features are consistent with phreatic surfaces of perched water bodies filling pore spaces or cavities in subsurface ice. Indeed, our in situ observations during other sensor installations consistently revealed the widespread presence of water or air-filled cavities 30–90 cm beneath the Channel Lake basin. The GPR observations of Type B features share some characteristics with firn aquifers observed in locations such as the Greenland Ice Sheet (Forster and others, 2013), Svalbard (Christianson and others, 2015) and the European Alps (Kullessa and others, 2008; Kullessa and others, in press), which are able to accommodate substantial meltwater flow and storage. However, our observed features are highly spatially constrained to the Channel Lake basin, and the lack of firn observed at the site requires a different explanation for the presence of subsurface cavities. One possibility is that subsurface porosity was created by a lake drainage event, as previously floating ice descended onto the underlying surface. An alternative explanation could be that the water was created directly by subsurface melting, a process which has been observed to occur in Antarctica when surface

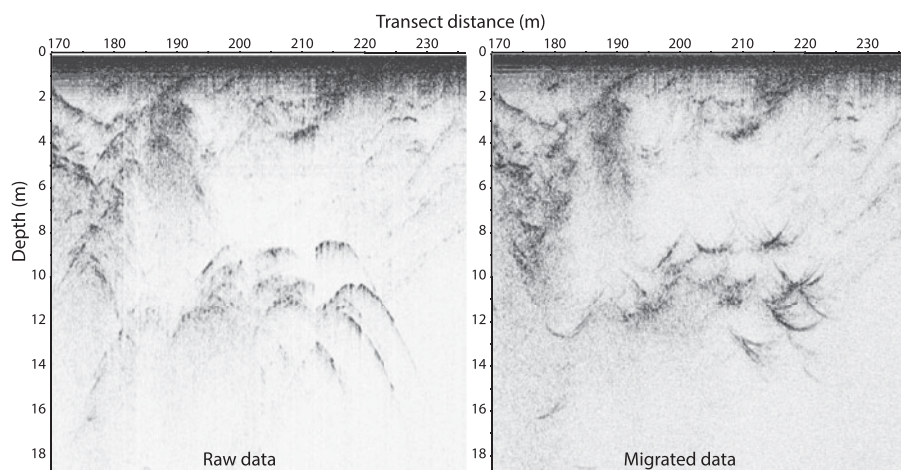


**Fig. 5.** Section of non-static-corrected 800 MHz GPR data from Line 1 that shows the characteristic diffractions of Type A features (left), and the migration effect, which attempts to collapse these diffractions to points. We infer that these point features represent englacial crevasses.

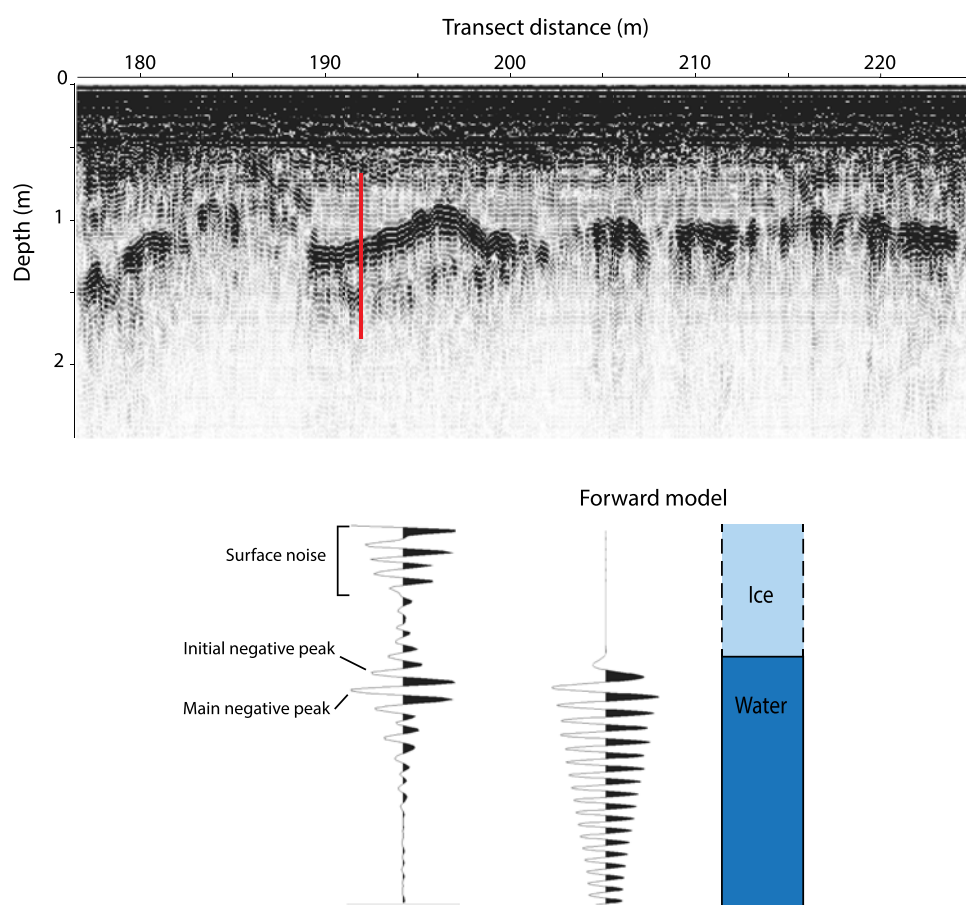


**Fig. 6.** Section of 800 MHz GPR data from Line 4 illustrating a typical Type B feature as a bright, shallow, horizontally extensive feature. Red line represents the extracted trace, which is compared against a forward model trace from an ice–water interface.

air temperatures are below zero and penetration of solar radiation allows melting of the ice at depth (Liston and others, 1999). Despite the more spatially constrained nature of our observations, surface meltwater ponds have been observed extensively around the coast of Antarctica (Kingslake and others, 2017) and this type of subsurface meltwater lens could have an important effect on the movement and storage of meltwater in Antarctica.

Comparing the forward modelling results to our GPR observations, most of the Type C englacial reflections in Sørsdal Glacier are bright and characterised by negative polarities (Fig. 7a), and are therefore consistent with the presence of ice–water interfaces – potentially indicating water-filled englacial voids at depths that

typically exceed 5 m (Fig. 4). Exceptionally, two large Type C features in Lines 1 and 4 (Fig. 7b) are characterised by a dimmer reflection with positive polarity above a brighter reflection with negative polarity. These observations are consistent with the presence of englacial voids containing pockets of air above water layers, the surfaces of which are likely to be flat in reality but appear to be undulating in our migrated images. These undulations are artefacts likely caused by off-line effects within the cone-shaped radar beam transmitted by our system, generated as our profiles cross voids at oblique angles (Arcone and Yankielun, 2000; Benn and others, 2017), and because small-scale differences in radar velocities are not accounted for in our 2-D migration

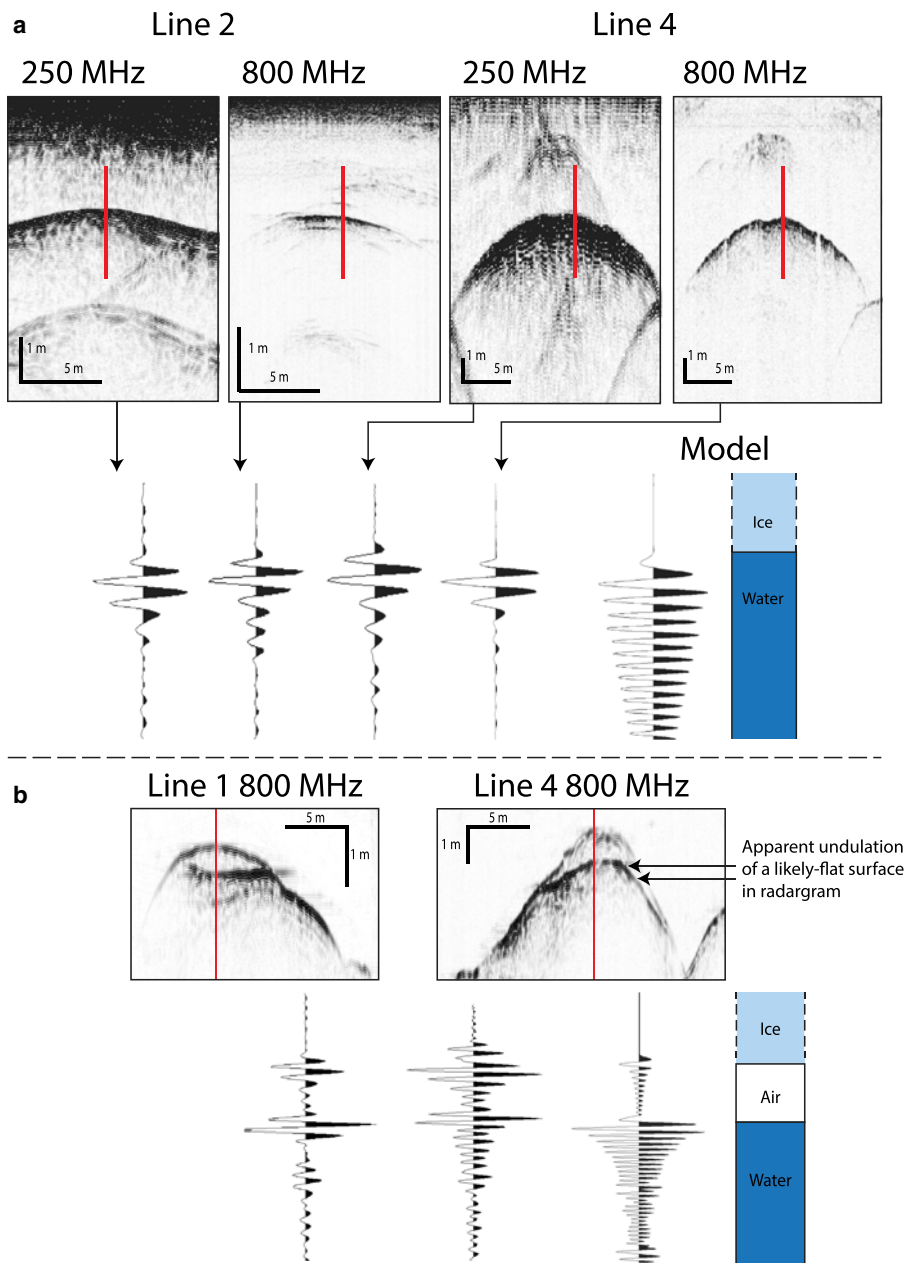


**Fig. 7.** (a) Radargrams and extracted traces showing the signal characteristics of Type C features, with ice–water forward model for comparison. (b) Radargrams and traces from two Type B features compared against an ice–air–water forward model trace. Note that the lower reflector, interpreted as the top of a water body in both features, is apparently undulating in the radargrams. This is likely a distorted view of a flat surface.

**Table 4.** Theoretical values of vertical resolution and skin depth for ice, water, and air for both 250 MHz and 800 MHz GPR antennas

Material	Vertical resolution (m)		Skin depth (m)	
	250 MHz	800 MHz	250 MHz	800 MHz
Ice	0.17	0.05	10.06	5.62
Water	0.03	0.01	1.42	0.80
Air	0.30	0.09	∞	∞

algorithm. Notwithstanding the undulations, we can infer that the travel time difference between the dimmer and brighter reflectors is consistent with air pockets thicker than 1 m at the centre location (marked by red lines in Fig. 7b). As expected, we also cannot delineate the base of the void beneath the water layer.

Our GPR observations on Sørsdal Glacier detected numerous Type C englacial features, which we can infer to be either water-filled or containing a water layer below an air pocket. It is possible that many of the features that appear as water-filled in our data do in fact contain an air pocket above the water layer, but that this air

pocket is so thin that we cannot distinguish it in our GPR data. The geometries of these Type C features, and the morphology of the Channel Lake itself point to a number of possible formation mechanisms.

Although we cannot assert the exact formation mechanism, we propose that the Channel Lake basin was probably formed by the drainage of a previous surface lake for three main reasons. First, the Channel Lake basin was a dry depression when we visited it in February 2017, but was observed to be water-filled in satellite imagery from previous years. During the time of our survey campaign, large volumes of water were in fact observed to pool in



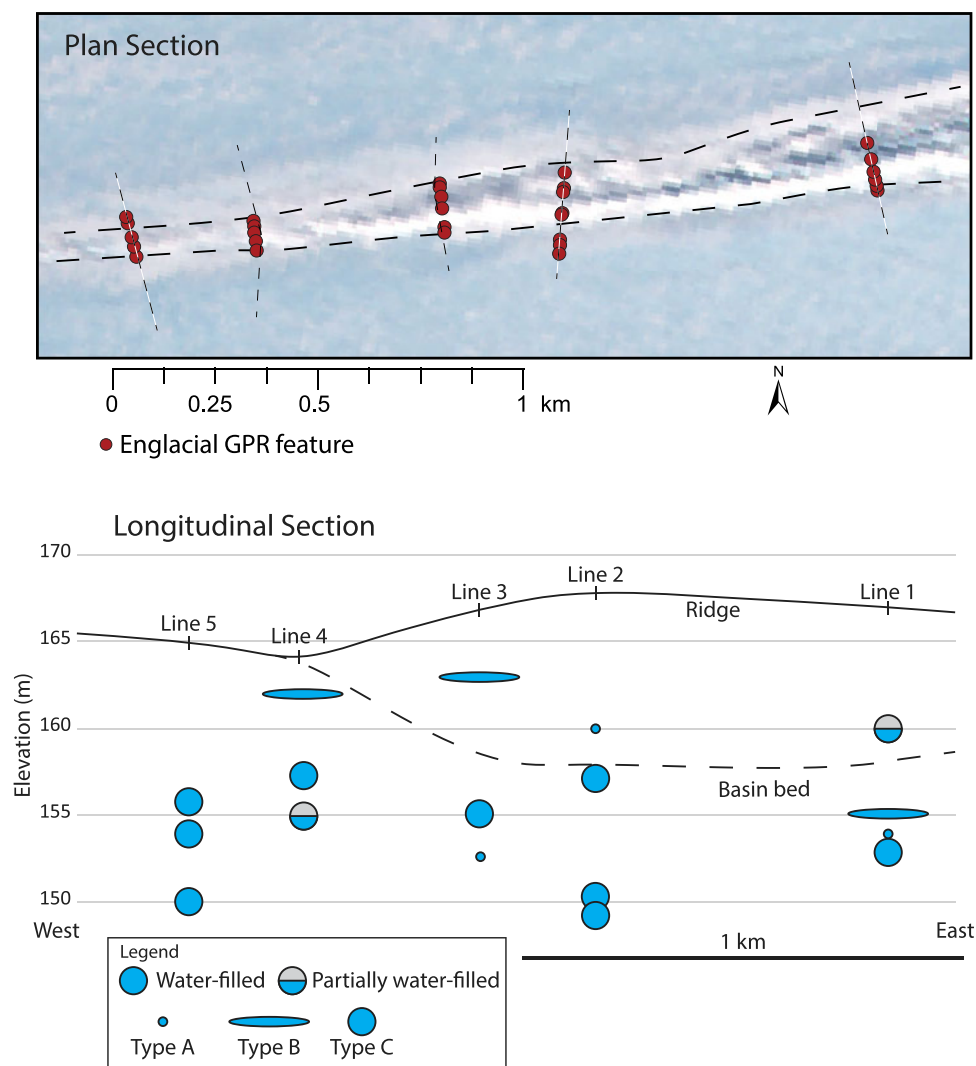


**Fig. 8.** Conceptualised image of hydrological features identified in our GPR data, classified by type (see text). Map locations of features shown at the top relative to Channel Lake, cross-sectional depth distribution of features shown irrespective of the horizontal location along any given profile line at bottom.

lakes on the glacier surface elsewhere. Second, the oval shape of the basin with crevassed margins is similar to depressions observed elsewhere in East Antarctica that were caused by surface lake drainage (Langley and others, 2016). Third, there are geomorphological similarities to previously-observed ice dolines, which form characteristically elongate and distinctive basins in otherwise flat surface ice (Bindschadler and others, 2002) although the edges of the Channel Lake are less sharply-defined.

We also propose that the Channel Lake basin was drained through the englacial pathways imaged by our GPR surveys. Based on similar observations, Stuart and others (2003) inferred the widespread presence of ponds of water in relict englacial pathways in the cold austre Brøggerbreen in Svalbard, which covered between 14 and 90% of the channel height. These inferences are directly compatible with our own observations at Sørødal Glacier, and it is therefore likely that any surface ablation during our survey periods was drained into and potentially through the englacial pathways we have imaged. Although Type C features are common in our data, the large spacing between our survey profiles (Fig. 1) makes it challenging to infer the potential presence of interconnected voids with any degree of certainty (Fig. 8). Future campaigns aiming to further characterise near-surface englacial features at Channel Lake and other sites may aim to provide a more detailed analysis, using closer spacing to delineate and potentially determine interconnectivity of features. Otherwise further

studies may seek to determine the spatial distribution of englacial features across the glacier and the rest of the Antarctic coast.

## Conclusions

Our GPR data acquired along sub-parallel profiles on Sørødal Glacier (Fig. 1) provide compelling evidence for the presence of englacial voids filled with water, or air pockets above water, at depths typically exceeding 5 m but <20 m (Type C features, Figs. 4 and 7). The data are furthermore consistent with lenses of meltwater held within porous ice at depths of <5 m, and perched on impermeable glacier ice, that are conceptually similar to the firn aquifers observed on the Greenland Ice Sheet, as well as the Arctic and Alpine glaciers. These englacial water bodies are observed adjacent to and more than 2 km downstream of a dry relict surface pond, which is consistent with pond drainage into an interconnected englacial drainage system. Indeed, entirely consistent with these inferences, a large early melt season outburst flood from this implied system was identified in 2016/17 satellite imagery.

Our observations imply that meltwater can be stored and possibly flow in shallow hydrological systems in East Antarctica, thus affecting the volume and timing of meltwater contribution to local surface mass balance, akin to processes inferred previously for the Greenland Ice Sheet (e.g. Forster and others, 2013). Future work



should therefore ascertain the spatial prevalence of such hydrological systems along the East Antarctic coastline, identify to what degree the meltwater is mobile and redistributed or refrozen and on what timescales, and quantify any impacts on surface mass-balance contributions.

**Acknowledgements.** Data collection was supported through the Australian Government's Australian Antarctic Science Grant Program under project AAS 4342. This work was supported by the Australian Government's Business Cooperative Research Centres Programme through the Antarctic Climate and Ecosystems Cooperative Research Centre (ACE CRC) and the Australian Research Council's Special Research Initiative for the Antarctic Gateway Partnership (project ID SR140300001). Landsat 8 imagery courtesy of the US Geological Survey. Thanks to Hugh Tassel and Will McAdam for providing advice and assistance in data processing.

## References

- Alley RB, Dupont TK, Parizek BR and Anandakrishnan S (2005) Access of surface meltwater to beds of sub-freezing glaciers: preliminary insights. *Annals of Glaciology* **40**, 8–14.
- Arcone SA and Yankielun NE (2000) 1.4 GHz radar penetration and evidence of drainage structures in temperate ice: Black Rapids Glacier, Alaska, U.S.A. *Journal of Glaciology* **46**(154), 477–490. doi: [10.3189/172756500781833133](https://doi.org/10.3189/172756500781833133).
- Banwell AF, MacAyeal DR and Sergienko OV (2013) Breakup of the Larsen B Ice Shelf triggered by chain reaction drainage of supraglacial lakes. *Geophysical Research Letters* **40**(22), 5872–5876.
- Benn D and 5 others (2017) Structure and evolution of the drainage system of a Himalayan debris-covered glacier, and its relationship with patterns of mass loss. *Cryosphere* **11**(5), 2247–2264. doi: [10.5194/tc-11-2247-2017](https://doi.org/10.5194/tc-11-2247-2017).
- Bindschadler R, Scambos TA, Rott H, Skvarca P and Vornberger P (2002) Ice dolines on Larsen Ice Shelf, Antarctica. *Annals of Glaciology* **34**, 283–290.
- Catania GA, Neumann TA and Price SF (2008) Characterizing englacial drainage in the ablation zone of the Greenland ice sheet. *Journal of Glaciology* **54**(187), 567–578.
- Christianson K, Kohler J, Alley RB, Nuth C and van Pelt WJJ (2015) Dynamic perennial firn aquifer on an Arctic glacier. *Geophysical Research Letters* **42**(5), 1418–1426. doi: [10.1002/2014gl062806](https://doi.org/10.1002/2014gl062806).
- da Rosa KK and 5 others (2014) Stratigraphy of Wanda Glacier, King George Island, Antarctica, using ground penetrating radar. *Revista Brasileira de Geofísica* **32**(1), 21–30.
- Das SB and 6 others (2008) Fracture propagation to the base of the Greenland Ice Sheet during supraglacial lake drainage. *Science* **320**(5877), 778–781.
- Doyle SH and 9 others (2013) Ice tectonic deformation during the rapid in situ drainage of a supraglacial lake on the Greenland Ice Sheet. *The Cryosphere* **7**(1), 129–140. doi: [10.5194/tc-7-129-2013](https://doi.org/10.5194/tc-7-129-2013).
- Forster RR and 12 others (2013) Extensive liquid meltwater storage in firn within the Greenland ice sheet. *Nature Geoscience* **7**, 95–98. doi: [10.1038/ngeo2043](https://doi.org/10.1038/ngeo2043).
- Fountain AG and Walder JS (1998) Water flow through temperate glaciers. *Reviews of Geophysics* **36**(3), 299–328. doi: [10.1029/97RG03579](https://doi.org/10.1029/97RG03579).
- Gulley JD, Benn DI, Screaton E and Martin J (2009) Mechanisms of englacial conduit formation and their implications for subglacial recharge. *Quaternary Science Reviews* **28**(19–20), 1984–1999. doi: [10.1016/j.quascirev.2009.04.002](https://doi.org/10.1016/j.quascirev.2009.04.002).
- Jones GA, Kulessa B, Doyle SH, Dow CF and Hubbard A (2013) An automated approach to the location of icequakes using seismic waveform amplitudes. *Annals of Glaciology* **54**(64), 1–9. doi: [10.3189/2013AoG64A074](https://doi.org/10.3189/2013AoG64A074).
- Kim KY, Lee J, Hong MH, Hong JK and Shon H (2010) Helicopter-borne and ground-towed radar surveys of the Fourcade Glacier on King George Island, Antarctica. *Exploration Geophysics* **41**(1), 51–60. doi: [10.1071/EG09052](https://doi.org/10.1071/EG09052).
- Kingslake J, Ely JC, Das I and Bell RE (2017) Widespread movement of meltwater onto and across Antarctic ice shelves. *Nature* **544**(7650), 349–352.
- Kulessa B, Booth AD, Hobbs A and Hubbard AL (2008) Automated monitoring of subglacial hydrological processes with ground-penetrating radar (GPR) at high temporal resolution: scope and potential pitfalls. *Geophysical Research Letters* **35**(24), L24502. doi: [10.1029/2008GL035855](https://doi.org/10.1029/2008GL035855).
- Kulessa B (in press) Seismoelectric characterisation of ice sheets and glaciers. In Grobbe N, Reil A, Zhu Z and Slob E ed. *Seismoelectric Exploration: Theory, Experiments and Applications*. AGU Books, Washington, DC, USA.
- Langley ES, Leeson AA, Stokes CR and Jamieson SSR (2016) Seasonal evolution of supraglacial lakes on an East Antarctic outlet glacier. *Geophysical Research Letters* **43**(16), 8563–8571. doi: [10.1002/2016GL069511](https://doi.org/10.1002/2016GL069511).
- Lenaerts JTM and 12 others (2016) Meltwater produced by wind–albedo interaction stored in an East Antarctic ice shelf. *Nature Climate Change* **7**, 58. doi: [10.1038/nclimate3180](https://doi.org/10.1038/nclimate3180).
- Liston G, Winther J, Bruland O, Elvehøy H and Sand K (1999) Below-surface ice melt on the coastal Antarctic ice sheet. *Journal of Glaciology* **45**(150), 273–285. doi: [10.3189/S0022143000001775](https://doi.org/10.3189/S0022143000001775).
- MacAyeal DR and Sergienko OV (2013) The flexural dynamics of melting ice shelves. *Annals of Glaciology* **54**(63), 1–10. doi: [10.3189/2013AoG63A256](https://doi.org/10.3189/2013AoG63A256).
- Mellor M (1960) Antarctic ice terminology: ice dolines. *Polar Record* **10**(64), 92. doi: [10.1017/S0032247400050786](https://doi.org/10.1017/S0032247400050786).
- Plewes LA and Hubbard B (2001) A review of the use of radio-echo sounding in glaciology. *Progress in Physical Geography* **25**(2), 203–236.
- Reynolds JM (2011) *An Introduction to Applied and Environmental Geophysics*, 2nd Edn. John Wiley & Sons, Chichester, UK.
- Rignot E, Mouginot J and Scheuchl B (2017) MEaSUREs InSAR-Based Antarctica Ice Velocity Map, Version 2. Boulder, Colorado USA. NASA National Snow and Ice Data Center Distributed Active Archive Center. doi: <https://doi.org/10.5067/D7GK8F5J8M8R>.
- Scambos T and 7 others (2009) Ice shelf disintegration by plate bending and hydro-fracture: satellite observations and model results of the 2008 Wilkins ice shelf break-ups. *Earth and Planetary Science Letters* **280** (1–4), 51–60.
- Schoof C (2010) Ice-sheet acceleration driven by melt supply variability. *Nature* **468**(7325), 803–806. doi: [10.1038/nature09618](https://doi.org/10.1038/nature09618).
- Shreve RL (1972) Movement of water in glaciers. *Journal of Glaciology* **11**(62), 205–214. doi: [10.3189/S002214300002219X](https://doi.org/10.3189/S002214300002219X).
- Stolt RH (1978) Migration by Fourier transform. *Geophysics* **43**(1), 23–48. doi: [10.1190/1.1440826](https://doi.org/10.1190/1.1440826).
- Stuart G, Murray T, Gamble N, Hayes K and Hodson A (2003) Characterization of englacial channels by ground-penetrating radar: an example from austre Brøggerbreen, Svalbard. *Journal of Geophysical Research: Solid Earth* **108**(11), EPM 7-1–EPM 7-13.
- van der Veen CJ (2007) Fracture propagation as means of rapidly transferring surface meltwater to the base of glaciers. *Geophysical Research Letters* **34**(1), L01501. doi: [10.1029/2006GL028385](https://doi.org/10.1029/2006GL028385).
- Vatne G (2001) Geometry of englacial water conduits, Austre Brøggerbreen, Svalbard. *Norsk Geografisk Tidsskrift* **55**(2), 85–93. doi: [10.1080/713786833](https://doi.org/10.1080/713786833).
- Vatne G and Irvine-Fynn TDL (2016) Morphological dynamics of an englacial channel. *Hydrology and Earth System Sciences* **20**(7), 2947–2964. doi: [10.5194/hess-20-2947-2016](https://doi.org/10.5194/hess-20-2947-2016).
- Ward SH and Hohmann GW (1987) Electromagnetic theory for geophysical applications. In Nabighian M ed. *Electromagnetic Methods in Applied Geophysics*. Society of Exploration Geophysicists, Tulsa, OK, USA, 131–311. doi: [10.1190/1.9781560802631.ch4](https://doi.org/10.1190/1.9781560802631.ch4).
- Weertman J (1973) Can a water-filled crevasse reach the bottom surface of a glacier. *IASH publ* **95**, 139–145.
- Zwally HJ and 5 others (2002) Surface melt-induced acceleration of Greenland ice-sheet flow. *Science* **297**(5579), 218–222. doi: [10.1126/science.1072708](https://doi.org/10.1126/science.1072708).